**Smart Structures and Systems**, *Vol. 34, No. 1 (2024) 1-8*
https://doi.org/10.12989/sss.2024.34.4.001


# A study on transmission line configuration for structural health monitoring using electromagnetic waves

Dongsoo Lee [1a], Dong-Ju Kim [1b], Jinwook Kim [1b], Jong-Sub Lee [1c] and Sang Yeob Kim*[2]

[1] *School of Civil, Environmental and Architectural Engineering, Korea University, 145, Anam-ro, Seongbuk-gu, Seoul 02841, Republic of Korea*
[2] *Department of Fire and Disaster Prevention, Konkuk University, 268, Chungwon-daero, Chungju-si, Chungcheongbuk-do, 27478, Republic of Korea*

(*Received May 17, 2024, Revised August 12, 2024, Accepted August 13, 2024*)

**Abstract.** Structural health monitoring (SHM) of concrete structures is necessary because structural safety is directly linked to life safety. This study proposes a transmission line configuration for SHM based on time domain reflectometry (TDR). For this purpose, six transmission lines consisting of electrical wires, rebars, and joints were prepared. The TDR waveforms were measured and analyzed in air and concrete using six transmission lines to select the most suitable configuration. A two-line wire with joints was selected as the optimal transmission line for SHM because it exhibited the highest sensitivity among the configurations. Experiments to apply SHM were performed on defective concrete blocks containing an optimal transmission line. The results showed that the defect locations in concrete were precisely investigated using TDR waveform analysis. The distances estimated from the TDR waveform were similar to the measured distances for the locations of the defects and joints in the concrete blocks. This study suggests that a transmission line consisting of two-line wires and joints may be an effective non-destructive evaluation tool for assessing the structural health of concrete.

**Keywords:** electromagnetic waves; non-destructive evaluation; structural health monitoring; time domain reflectometry; transmission line

## 1. Introduction

Concrete has been the most widely used material in modern construction since Portland cement was invented by Joseph Aspidin in 1824 (Babor *et al*. 2009). Concrete is cheap and strong and can also form complex shapes due to its flowability before curing (Fowler 1999). Furthermore, the strength and durability of concrete can be controlled using various combinations of granular materials, as the concrete properties depend on the characteristics of the mixed materials (Armaghani *et al*. 1992). These advantages enable concrete to be used as the primary construction material in various types of infrastructures, leading to an increase in the number of concrete structures over time. However, defects often occur in concrete in the form of voids, which threaten the safety of structures (Chai *et al*. 2010). For safety and maintenance reasons, various testing methods have been developed and suggested for the evaluation of concrete. As the destructive methods, drilled core test (ASTM C42 2017) and penetration resistance test (ASTM C803 2017) have been used to measure the strength of the cast-in-place concrete. Although destructive methods can directly evaluate the material properties of structures, non-destructive methods are preferred because destructive methods may affect structural safety.

Structural health monitoring (SHM), a term encompassing various integrity test methods, is a non-destructive method for evaluating structural health using onboard sensors (Güemes *et al*. 2020). Various fields, such as aerospace, mechanical, and civil engineering, have employed structural health monitoring for damage identification (Farrar and Worden 2007, Kim *et al*. 2023b, Kong *et al*. 2021, Liu *et al*. 2023b, Tacim *et al*. 2023, Xuan *et al*. 2023). Previous studies used elastic or electromagnetic wave techniques (Kim *et al*. 2021b, 2023a, Yu *et al*. 2021, Hoang *et al*. 2022, Liu *et al*. 2023a). Farrar *et al*. (2001) identified structural damage using vibration methods with accelerometers. Jiao *et al*. (2016) investigated the fatigue cracks in metals employing an eddy current sensor. Structural monitoring has been attempted in civil engineering using time domain reflectometry (TDR). The TDR is generally used to evaluate the water content of soil in geotechnical engineering (Kim *et al*. 2016, 2021a, Park *et al*. 2023). However, only a few studies have employed TDR as a monitoring technique for particular structures. Lin *et al*. (2009) developed a concrete column involving a TDR sensor to monitor landslides. Yu *et al*. (2020b) performed bridge scour monitoring by observing the changes in TDR signals. Studies assessing the structural health of concrete have been conducted employing transmission line sensors. Lee *et al*. (2018) investigated the integrity of concrete piles

*Corresponding author, Ph.D., Assistant Professor,
E-mail: sangyeob@kku.ac.kr
[a] Postdoctoral Research Associate
[b] Ph.D. Student
[c] Professor



ISSN: 1738-1584 (Print), 1738-1991 (Online)

by comparing the electromagnetic wave velocities in defective and sound concretes. However, transmission line type sensors have a problem because it is difficult to identify the size and location of defects in concrete.

An improved transmission line configuration was suggested to solve this problem. A transmission line generally comprises two conductors adopted as the signal and return paths (Lee *et al*. 2020, Yu *et al*. 2020a, Lee *et al*. 2023). In reinforced concrete, a transmission line comprises rebars, or electrical wires preinstalled in the structure. Although the integrity of concrete can be assessed regardless of the combination of the rebar and wire, the TDR waveform changes with the combination. This change in the waveform is due to an electromagnetic wave signal influenced by the characteristic impedance. The characteristic impedance of the transmission line varies with its configuration. Based on the impedance change, Lee *et al*. (2024b) developed a transmission line containing artificial joints to identify the defect type and the size and location of defects in concrete. Artificial joints function as reference points in TDR waveform but their properties are also affected by the characteristic impedance. However, studies on transmission line configurations with artificial joints are limited.

This study aims to investigate the optimal transmission line configuration for TDR-based SHM to evaluate concrete structures. This paper explains the principle and measurement system of SHM based on TDR. Subsequently, experiments for the transmission line configuration are addressed. The properties of the waveform depending on the transmission line configuration are explained. The experimental results for SHM are described when applied to model blocks with an optimal transmission line configuration. Finally, the SHM results applied to the two defective blocks are analyzed and discussed.

## 2. Experimental setup

### *2.1 Structural health monitoring based on TDR*

TDR measures the quantity of electromagnetic waves reflected along the transmission line (Noborio *et al*. 1996). TDR records the reflection coefficient or voltage of the reflected electromagnetic wave with travel time. The amplitude of electromagnetic waves depends on the impedance of the transmission line, whereas the velocity of electromagnetic waves varies with the dielectric permittivity (Lee *et al*. 2024a). These properties allow structural health monitoring (SHM) using TDR. Fig. 1 shows an example of a TDR waveform measured in a concrete structure using a transmission line with an artificial joint. The X-axis represents time, and the Y-axis shows the recorded amplitude of the electromagnetic wave. The amplitude can be expressed as a reflection coefficient (Γ) or voltage, and the relationship is as follows

$$\Gamma = \frac{V_o}{V_i} \tag{1}$$

where $V_o$ denotes the output voltage returning to the time

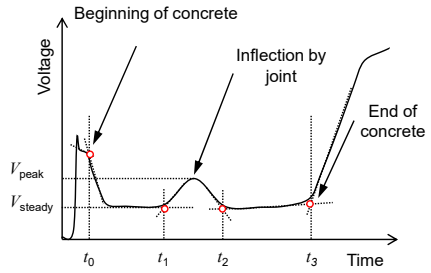


Fig. 1 Example of TDR waveform in concrete using transmission line with joint

domain reflectometer (TDR unit), and $V_i$ represents the input voltage generated by the TDR unit. The input voltage is a constant value determined by the TDR unit, whereas the output voltage changes with the transmission line conditions. The transmission line conditions cause a variation in the characteristic impedance, which is related to the reflection coefficient as follows

$$\Gamma = \frac{Z_2 - Z_1}{Z_2 + Z_1} \tag{2}$$

where $Z_1$ and $Z_2$ denote the characteristic impedances of media 1 and 2, respectively. Because the amplitude of the wave changes with the characteristic impedance of the transmission line, inflections occur at the beginning and end of the concrete. The joint affects the waveform for the same reason; it can be used as a reference point to identify the location corresponding to time. The electromagnetic wave velocity ($v$) can be estimated using the time at the inflection points and the travel distance using the following equation

$$v = \frac{d}{\Delta t} \tag{3}$$

where $d$ denotes the travel distance, $\Delta t$ is the time difference between the two inflection points. The permittivity and permeability of medium-propagating electromagnetic waves determine their wave velocities. In civil engineering, the magnetic permeability is assumed to be 1, identical to that in free space (Topp *et al*. 1980). Therefore, permittivity and velocity have the following relationships

$$v = \frac{c}{\sqrt{\varepsilon_r}} \tag{4}$$

where $c$ and $\varepsilon_r$ denote the electromagnetic wave velocity in free space and the relative permittivity of the medium, respectively. Note that the relative permittivity of air is approximately 1, and that of concrete is 4 – 10 (Rhebergen *et al*. 2002). Thus, the difference in the relative permittivity enables the use of the TDR-based method to evaluate the structural health of concrete. Furthermore, the time at the inflection point of the joint allows location estimation in the waveform.

### *2.2 Measurement system*

Fig. 2 presents the measurement system for structural

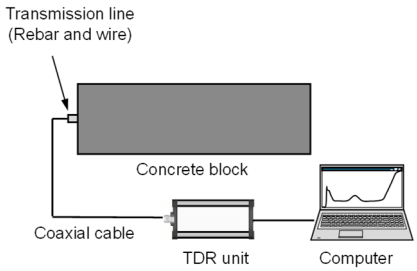


Fig. 2 Measurement system

health monitoring using TDR. A TDR unit was used to generate and measure electromagnetic wave signals. The signals generated by the TDR unit were transmitted through a coaxial cable (RG-316) to protect the wave signals from electrical noise. The coaxial cable was connected to a transmission line consisting of a rebar and a preinstalled electrical wire. The signals were stacked 256 times to reduce measurement error, and the input voltage of the signals was 250 mV. The transmission line monitored the structural health of the concrete block by analyzing the electromagnetic wave velocity and signal amplitude.

The transmission line is composed of two conductors: the signal and return paths. In this study, the six transmission lines consisted of two electrical wires or one wire and a rebar. All transmission line (TL) configurations used in this study are listed in Table 1. TL 1, 2, 3, and 4 consisted of one wire and one rebar, whereas TL 5 and 6 only used electrical wires. All the configurations had an artificial joint in the middle of the transmission line. For TL 1, a single electrical wire (60227-KS IEC 02) was used for the signal path and was combined with the rebar used for the return path. TL 2, 3, and 4 used one line of a two-line electrical wire (60227-KS IEC, VFF) as the signal path and employed a rebar as the return path. In the case of TL 5 and 6, two-line electrical wires were employed as transmission lines that did not require rebars. The TDR waveforms were measured in air and concrete for all configurations to evaluate the transmission line characteristics. A concrete block with six types of embedded transmission lines is illustrated in Fig. 3. The block was 150 cm long, 40 cm wide, and 60 cm high. Six D16 rebars were placed in sufficient space (length, 17 cm; width, 15 cm) to prevent mutual interference. Electrical wires were attached to the rebars for the transmission line configuration.

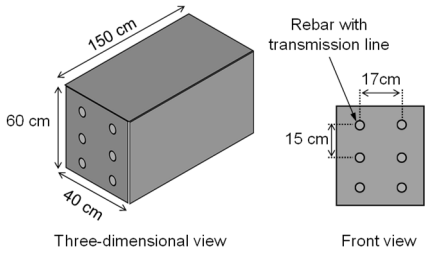


Fig. 3 Concrete block with six types of embedded transmission lines

## 3. Experimental study

### *3.1 Optimal transmission line verification*

#### *3.1.1 Waveform observation in air*

Experiments were conducted to determine an optimal transmission line. Fig. 4 shows the TDR waveforms measured using different transmission line configurations in air. In the waveforms, inflections at the beginning and end of the transmission lines are observed for all the configurations. The output voltage of waves reflected in air ranges from 55.29 to 77.50 mV for transmission lines consisting of one wire with rebar (TL 1, 2, 3, and 4). Transmission lines consisting of two-line electrical wires (TL 5 and 6) show a voltage higher than 100 mV, which is higher than that in a single wire with a rebar. On the other hand, inflections by joints occur, and in some cases, inflection is difficult to observe owing to its low amplitude. The average voltage of TL 1 in the air is 55.29 mV, while the peak voltage in the inflection caused by the joint is 78.26 mV. For TL 2, the average voltage is approximately 77.53, and the peak voltage of the joint was 91.85. The voltage difference is attributed to the wire, as the only distinction between TL 1 and 2 is the wire type used for the signal path. Therefore, the impedance of a single electrical wire may be lower than that of a single line separated from a two-line wire. In the waveform for TL 3, the average and peak voltages are 73.21 mV and 83.77 mV, respectively. However, the inflection caused by the joint is difficult to distinguish in the waveform. The change in the waveform is insensitive due to the properties of the connector employed as the joint in TL 3. The waveform of TL 4 presented an average voltage of 66.95 mV. In contrast, TL 4 used a coaxial cable as an artificial joint, resulting in a lower voltage than the average. Thus, instead of the peak voltage, a trough voltage of approximately 53.34 mV is observed in the inflection caused by the joint. TL 5 which uses a two-

Table 1 Configurations of transmission line with joint

| Configuration | Signal path | Return path | Joint |
|---|---|---|---|
| TL 1 | 60227-KS IEC 02 | Rebar | single-line wire connector |
| TL 2 | 60227-KS IEC, VFF | Rebar | single-line wire connector |
| TL 3 | 60227-KS IEC, VFF | Rebar | Tube type connector |
| TL 4 | 60227-KS IEC, VFF | Rebar | Coaxial cable (RG58) |
| TL 5 | 60227-KS IEC, VFF | 60227-KS IEC, VFF | Two-line wire connector |
| TL 6 | 60227-KS IEC, VFF | 60227-KS IEC, VFF | 2 × single-line wire connector |

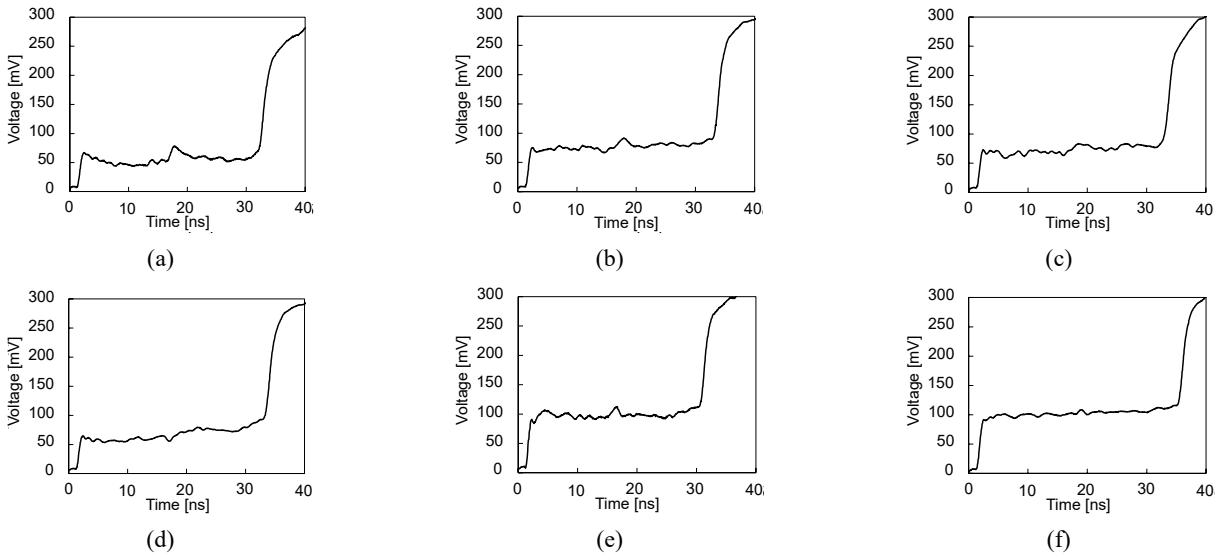


Fig. 4 TDR waveform of transmission lines in air: (a) TL 1; (b) TL 2; (c) TL 3; (d) TL 4; (e) TL 5; (f) TL 6

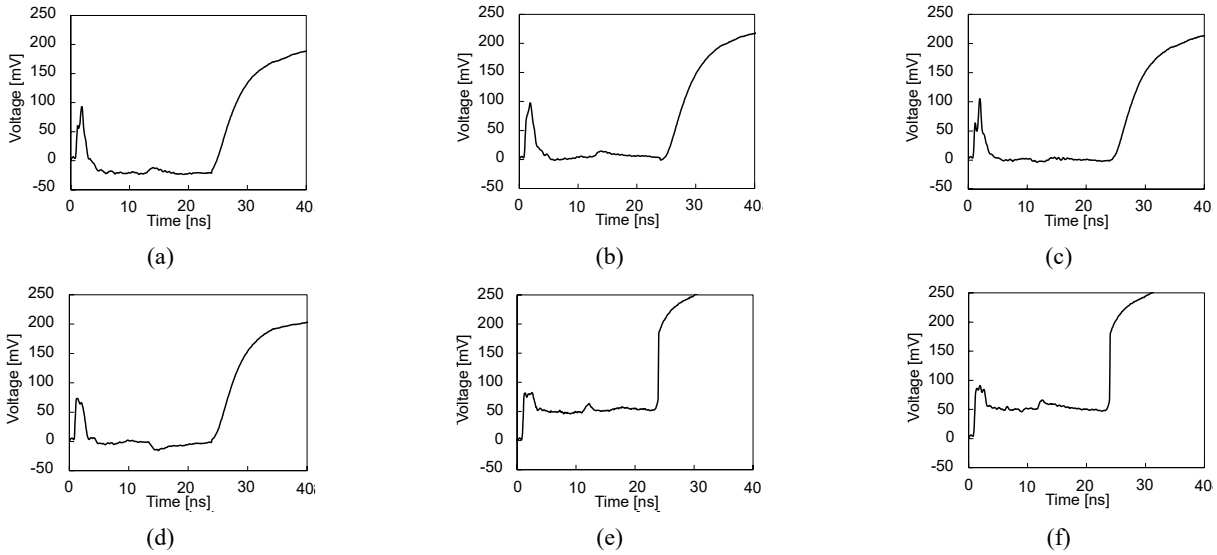


Fig. 5 TDR waveform of transmission lines in concrete block: (a) TL 1; (b) TL 2; (c) TL 3; (d) TL 4; (e) TL 5; (f) TL 6

line electrical wire as the signal and return path, has a higher average voltage (102.77 mV) than that of TL 1 – 4. The peak voltage in the inflection by the joint is approximately 110.82 mV. TL 6 shows an average voltage similar to that of TL 5 because of the same path configuration. The average voltage is 102.21 mV, whereas the peak voltage is 112.68 mV.

### *3.1.2 Waveform observation in concrete*

Experiments were conducted to observe the waveform characteristics of the concrete. All the transmission lines were embedded in the concrete block (see Fig. 3), and the TDR waveforms were measured after 28 days of curing period. Fig. 5 shows the TDR waveforms in the concrete for the transmission lines. Similar to the waveforms in air, the beginning and end of the concrete can be identified by inflections in the waveforms. For the transmission lines combining the wire and rebar (TL 1, 2, 3, and 4), the inflections at the beginning of the concrete show a sharp shape in the waveforms. Furthermore, the average voltages in the concrete are almost 0 mV, which is lower than those measured in air. In the case of the two-line wire type (TL 5 and 6), the inflections at the beginning of the concrete are blunt compared to those of the single wire with rebar (TL 1, 2, 3, and 4). The average voltage of TL 1 in the concrete shows the lowest value among the transmission lines, approximately -18.79 mV, while the peak voltage in inflection by joint is 3.37 mV. This is because the transmission line consists of a single wire with a rebar and has a lower impedance than the other transmission lines. For the waveform of TL 2, The average and peak voltages are 5.51 and 8.35 mV, respectively. In the waveform of TL 3, the average voltage is 0.67 mV, and the peak voltage is 4.05 mV. The inflection by the joint is difficult to discern because of its low amplitude and slow response. Because TL 4 uses a coaxial cable type artificial joint, a trough


Fig. 6 Sensitivity of transmission lines with different configurations: (a) in air; (b) in concrete

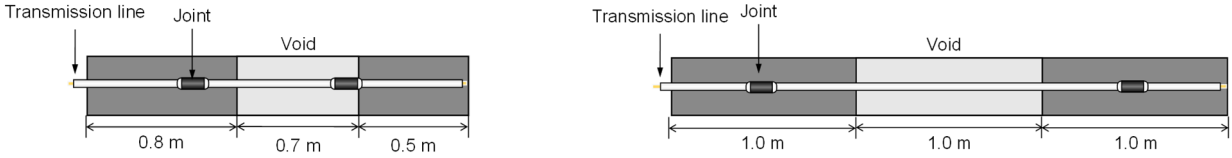


Fig. 7 Two different concrete blocks involving transmission line with joint:
(a) case 1: joint located defect region; (b) case 2: joint located sound region

inflection is observed in the waveform. The average voltage in concrete is 7.38 mV; the trough voltage is -5.57 mV. For waveforms measured by TL 5 and 6, the average voltages are 53.31 and 53.41 mV, while the peak voltages are 63.82 and 66.05 mV. The artificial joint employed in TL 5 shows a high amplitude in a short travel time, indicating a fast response. However, after inflection by the joint, the time to converge to the average voltage is gradual and slow in the waveform of TL 6.

### *3.1.3 Sensitivity evaluation*

The characteristics of transmission lines vary with the type of artificial joint and the condition of the signal and return paths. Although the characteristic impedance of a transmission line is an important factor, it is difficult to determine because it is affected by the surrounding material. According to a previous study, the inflection at a joint enables an indirect investigation of the transmission line properties (Lee *et al*. 2024b). The amplitude of electromagnetic waves attenuates with the propagation distance (Barrow 1936). Thus, observing the joint in the waveform is a reasonable method for selecting the most suitable transmission line configuration. In this section, quantitative comparisons are performed by analyzing the TDR waveforms. For quantitative analysis, we suggest the "Sensitivity" related to the rise and fall time of inflections and amplitude. The amplitude ($\Delta V$) and time interval ($\Delta t_J$) at the inflection point of the joint (see Fig. 1) are defined as follows

$$\Delta V = V_{peak} - V_{steady} \tag{5}$$

$$\Delta t_J = t_2 - t_1 \tag{6}$$

The sensitivity of the transmission line can be defined by the values computed using Eqs. (5) and (6), as follows

$$S = \frac{\Delta V / V_i}{\Delta t_J / t_T} = \frac{(V_{peak} - V_{steady}) \cdot t_T}{V_i \cdot (t_2 - t_1)} \tag{7}$$

where $V_i$ is the input voltage (250 mV). $t_T$ is the time difference between $t_0$ and $t_3$, the travel time in the transmission line. Thus, the sensitivity of the transmission line, depending on the configuration, is quantitatively computed.

Fig. 6 shows the sensitivity of the transmission lines with different configurations. When the transmission lines are in the air, the sensitivity of TL 1 shows the highest value (0.74), whereas it decreases to 0.19 in concrete. Because TL 1 consists of a rebar and a single electrical wire with a small cross-sectional area, the influence of the surrounding material may be greater than that of TL 2 and 3. For TL 2 and 3, the sensitivities in air are 0.62 and 0.37, respectively, which decrease to 0.15 and 0.13 in concrete. In contrast, TL 4, which employs a coaxial cable as a joint, is shown to be less affected by the surrounding medium, owing to a small decrease in sensitivity from 0.45 in air to 0.35 in concrete. Two-wire type transmission lines, TL 5 and TL 6 exhibit high sensitivity to both air and concrete. For TL 5, the sensitivities in air and concrete are 0.65 and 0.41, respectively. The sensitivities of TL 6 are 0.57 in air and 0.27 in concrete. In this study, TL 5 is selected as the optimal transmission line configuration because the sensitivity in concrete is more critical than that in air.

## *3.2 Model test for application*

### *3.2.1 Defective concrete model*

Defective concrete blocks were prepared to evaluate the applicability of the optimal transmission line configuration (TL 5). Two different concrete blocks involving a transmission line with joints are shown in Fig. 7. Two concrete blocks were used to simulate the defect regions containing the joints. The cross-sectional area of concrete blocks was 0.2 m × 0.2 m. For case 1 (Fig. 7(a)), the length of the concrete block was 2.0 m; the transmission line involved two artificial joints positioned at 0.67 and 1.33 m. One artificial joint was exposed to air because the void (defect region) was located from 0.8 to 1.5 m of the

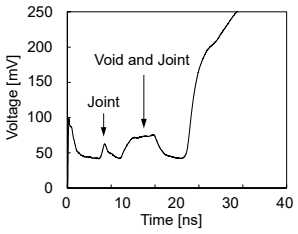


(a)

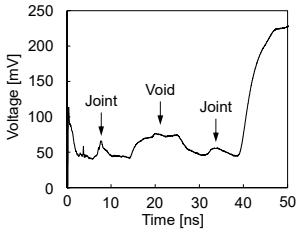


(b)

Fig. 8 TDR waveform measured in concrete block using transmission line with joint: (a) case 1; (b) case 2

concrete block. For case 2 (Fig. 7(b)), the concrete block was 3.0 m long and equally divided into three sections. Two artificial joints were installed at 0.5 and 2.5 m in each concrete section, while the void section didn't contain a joint. The TDR waveforms were measured for each concrete block.

### *3.2.2 Waveform observation*

The TDR waveforms measured in the concrete blocks are presented in Fig. 8. The beginning and end of the concrete are observed in the waveforms. Fig. 8(a) shows the TDR waveform for Case 1, one of the joints located in the void. The joint located at 0.67 m occurs inflection, which is detected in the waveform, whereas the second joint at 1.33 m is shrouded in inflection by void defect. In contrast, the TDR waveform for Case 2 (Fig. 8(b)) presents inflections caused by the joints and void defect. The inflection by the second joint located at 2.5 m exhibits a lower amplitude than that of the first joint owing to the attenuation of the electromagnetic waves. Electromagnetic waves exponentially attenuate with propagation distance, as follows (Kwak *et al*. 2016)

$$E_L = E_i \cdot e^{-\alpha L} \tag{8}$$

where $E_L$ and $E_i$ represent the amplitudes at distance L and the initial amplitude, respectively. $\alpha$ denotes the attenuation factor, a function of the conductivity and permittivity (Dalton *et al*. 1984). $\alpha$ is calculated to be 0.15 based on the amplitude of the joints. The sensitivity of the joint decreases from 0.82 at the first to 0.26 at the second.

### *3.2.3 Simulate analysis of waveform*

Assuming that the waveforms were acquired in the construction field, they were analyzed to identify the defects occurring in concrete structures. From the waveforms, the locations of the joints and the time between inflection points allow us to compute the electromagnetic wave velocity. The electromagnetic wave velocity is about $1.51 - 1.52 \times 10^8$ m/s in concrete, while the wave velocity in air (void) is approximately $1.96 \times 10^8$ m/s. Based on the wave velocity in the concrete and air, the locations of the defects are estimated using the time between the inflection points. For case 1, the location of the joint is computed at 0.63 m from the beginning of the concrete. The defect is estimated to range from 0.81 m to 1.55 m. For case 2, the locations of joints are estimated to be 0.51 m and 2.46 m. The void defect is evaluated to range from 0.98 m to 2.01 m. Fig. 9 presents a comparison between the estimated and

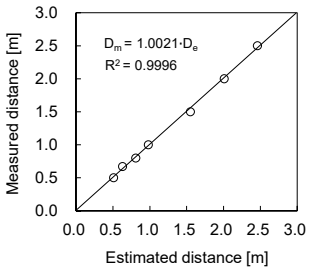


Fig. 9 Comparison between estimated distance and measured distance

measured distance of joint and defect from reference points. The measured distances are slightly larger than the estimated distances; however, the regression analysis shows a linear relationship with a determinant coefficient of 0.9996. Therefore, SHM based on TDR can be used to evaluate structural defects using an appropriate transmission line configuration.

## 4. Conclusions

This study investigated the optimal transmission line configuration for TDR-based SHM to evaluate concrete structures. Six different transmission lines were configured using rebars, electrical wires, and artificial joints. The TDR waveforms for the configured transmission lines were observed and analyzed in air and concrete. The optimal transmission line was selected using a sensitivity analysis. To evaluate the suitability of SHM, two defective concrete blocks involving the optimal transmission line were prepared. SHM was performed on the defective concrete blocks. The defect locations and sizes were estimated and compared with the measured values. The conclusions of this study are as follows:

- The sensitivity of transmission lines varies with the configuration owing to the transmission line's characteristic impedance. Transmission lines consisting of two-line wires were evaluated as better sensors than those configured with rebar and single wires.
- Joints and defects occurring in the concrete were observed in the TDR waveform. However, the sensitivity decreased with distance owing to attenuation. The attenuation of the electromagnetic waves was computed using the attenuation equation

and wave amplitude at the joints.

- The defect locations in concrete were precisely investigated using TDR waveform analysis. The estimated distances were similar to the measured distances for the locations of the defects and joints in the concrete blocks.
- Further studies are required to focus on the spacing and influence range of transmission lines. A transmission line consisting of two-line wires and joints could then serve as a robust, non-destructive evaluation tool for assessing the structural health of concrete.

## Acknowledgments

This work was supported by the Technology Innovation Program (P0024559, AI based Safety Assessment and Management System for Concrete Structures) funded by the Ministry of Trade, Industry & Energy (MOTIE, Korea).

## References

Armaghani, J.M., Larsen, T.J. and Romano, D.C. (1992), "Aspects of concrete strength and durability", *Transport. Res. Rec.*, (1335).

ASTM C42 (2017), Standard Test Method for Obtaining and Testing Drilled Cores and Sawed Beams of Concrete; ASTM International, West Conshohocken, PA, USA.

ASTM C803 (2017), Standard Test Method for Penetration Resistance of Hardened Concrete; ASTM International, West Conshohocken, PA, USA.

Babor, D., Plian, D. and Judele, L. (2009), "Environmental impact of concrete", *Buletinul Institutului Politehnic din lasi*, *Sectia Constructii*, *Arhitectura*., **55**(4), 27.

Barrow, W. (1936), "Transmission of electromagnetic waves in hollow tubes of metal", *Proc. Inst. Radio Eng.*, **24**(10), 1298-1328. http://doi.org/10.1109/JRPROC.1936.227357

Chai, H.-Y., Phoon, K.-K. and Zhang, D.-J. (2010), "Effects of the source on wave propagation in pile integrity testing", *J. Geotech Geoenviron. Eng.*, **136**(9), 1200-1208. https://doi.org/10.1061/(ASCE)GT.1943-5606.0000272

Dalton, F., Herkelrath, W., Rawlins, D. and Rhoades, J. (1984), "Time-domain reflectometry: Simultaneous measurement of soil water content and electrical conductivity with a single probe", *Sci.*, **224**(4652), 989-990. http://doi.org/ 10.1126/science.224.4652.989

Farrar, C.R. and Worden, K. (2007), "An introduction to structural health monitoring", *Philos. Trans. R. Soc. A-Math. Phys. Eng. Sci.*, **365**(1851), 303-315. https://doi.org/10.1098/rsta.2006.1928

Farrar, C.R., Doebling, S.W. and Nix, D.A. (2001), "Vibration–based structural damage identification", *Philos. Trans. R. Soc. Lond. Ser. A-Math. Phys. Eng. Sci.*, **359**(1778), 131-149. https://doi.org/10.1098/rsta.2000.0717

Fowler, D.W. (1999), "Polymers in concrete: a vision for the 21st century", *Cem. Concrete Compos.*, **21**(5-6), 449-452. https://doi.org/10.1016/S0958-9465(99)00032-3

Güemes, A., Fernandez-Lopez, A., Pozo, A.R. and Sierra-Pérez, J. (2020), "Structural health monitoring for advanced composite structures: a review", *J. Compos. Sci.*, **4**(1), 13. https://doi.org/10.3390/jcs4010013

Hoang, N.Q., Kim, S.Y. and Lee, J.-S. (2022), "Compressibility, stiffness and electrical resistivity characteristics of sand–diatom mixtures", *Géotechnique*, **72**(12), 1068-1081. https://doi.org/10.1680/jgeot.20.P.136

Jiao, S., Cheng, L., Li, X., Li, P. and Ding, H. (2016), "Monitoring fatigue cracks of a metal structure using an eddy current sensor", *EURASIP J. Wirel. Commun. Netw.*, **2016**, 1-14. https://doi.org/10.1186/s13638-016-0689-y

Kim, S.Y., Hong, W.-T., Hong, S.S., Baek, Y. and Lee, J.-S. (2016), "Unfrozen water content and unconfined compressive strength of frozen soils according to degree of saturations and silt fractions", *J. Korean Geotech. Soc.*, **32**(12), 59-67. https://doi.org/10.7843/kgs.2016.32.12.45

Kim, S.Y., Kim, Y. and Lee, J.-S. (2021a), "Effects of frozen water content and silt fraction on unconfined compressive behavior of fill materials", *Constr. Build. Mater.*, **266**, 120912. https://doi.org/10.1016/j.conbuildmat.2020.120912

Kim, S.Y., Park, J. and Lee, J.-S. (2021b), "Coarse-fine mixtures subjected to repetitive Ko loading: Effects of fines fraction, particle shape, and size ratio", *Powder Technol.*, **377**, 575-584. https://doi.org/10.1016/j.powtec.2020.09.017

Kim, S.Y., Chun, J.K., Yeo, J.Y. and Lee, J.-S. (2023a), "Estimation of soil porosity in mine tailing using parameters from instrumented oedometer test", *Eng. Geol.*, **317**, 107065. https://doi.org/10.1016/j.enggeo.2023.107065

Kim, S.Y., Kwon, D.Y., Jang, A., Ju, Y.K., Lee, J.-S. and Hong, S. (2023b), "A review of UAV integration in forensic civil engineering: From sensor technologies to geotechnical, structural and water infrastructure applications", *Measurement*, **224**, 113886. https://doi.org/10.1016/j.measurement.2023.113886

Kong, S.-M., Oh, D.-W., Lee, S.-Y., Jung, H.-S. and Lee, Y.-J. (2021), "Analysis of reinforced retaining wall failure based on reinforcement length", *Int. J. Geo-Eng.*, **12**, 1-14. https://doi.org/10.1186/s40703-021-00143-6

Kwak, K., Park, D., Chung, W.K. and Kim, J. (2016), "Underwater 3-D spatial attenuation characteristics of electromagnetic waves with omnidirectional antenna", *IEEE-ASME Trans. Mechatron.* **21**(3), 1409-1419. http://doi.org/ 10.1109/TMECH.2015.2509466

Lee, J.-S., Song, J.U., Hong, W.-T. and Yu, J.-D. (2018), "Application of time domain reflectometer for detecting necking defects in bored piles", *NDT E Int.*, **100**, 132-141. https://doi.org/10.1016/j.ndteint.2018.09.006

Lee, J.-S., Yu, J.-D., Han, K. and Kim, S.Y. (2020), "Strength characteristics of sand–silt mixtures subjected to cyclic freezing-thawing-repetitive loading", *Sensors*, **20**(18), 5381. https://doi.org/10.3390/s20185381

Lee, D., Lee, J.-S., Byun, Y.-H. and Kim, S.Y. (2023), "Application of optimized time domain reflectometry probe for estimating contaminants in saline soil", *Geomech. Eng., Int. J.*, **33**(3), 291-299. https://doi.org/10.12989/gae.2023.33.3.291

Lee, D., Lee, J.-S., Ju, Y.K. and Byun, Y.-H. (2024a), "Advanced electromagnetic wave-based method for characterizing defects in cement-based structures using time domain reflectometry", *Comput. Concrete, Int. J.*, **33**(5), 621-630. https://doi.org/10.12989/cac.2024.33.5.621

Lee, D., Yu, J.-D., Jeong, S., Park, G. and Lee, J.-S. (2024b), "Non-destructive method for evaluating local integrity of model piles using electromagnetic waves", *NDT E Int.*, **141**, 102999. https://doi.org/10.1016/j.ndteint.2023.102999

Lin, C.-P., Tang, S.-H., Lin, W.-C. and Chung, C.-C. (2009), "Quantification of cable deformation with time domain reflectometry—implications to landslide monitoring", *J. Geotech. Geoenviron. Eng.*, **135**(1), 143-152. https://doi.org/10.1061/(ASCE)1090-0241(2009)135:1(143)

Liu, Y., Bai, Y., Gao, G. and Su, S. (2023a), "Acoustic emission localization in concrete using a wireless air-coupled monitoring system", *Smart Struct. Syst., Int. J.*, **32**(4), 195-205.

https://doi.org/10.12989/sss.2023.34.4.195
Liu, Z.-J., Wang, H.-B., Ma, Z., Ni, Y.-Q., Jiang, J., Sun, R. and Zhu, H.-W. (2023b), "Towards high-accuracy data modelling, uncertainty quantification and correlation analysis for SHM measurements during typhoon events using an improved most likely heteroscedastic Gaussian process", *Smart Struct. Syst., Int. J.*, **32**(4), 267-279. https://doi.org/10.12989/sss.2023.32.4.267
Noborio, K., McInnes, K. and Heilman, J. (1996), "Measurements of soil water content, heat capacity, and thermal conductivity with a single TDR probe1", *Soil Sci.*, **161**(1), 22-28.
O'Connor, K.M. and Dowding, C.H. (2021), *Geomeasurements by pulsing TDR cables and probes*, CRC Press, FL, USA.
Park, G., Kim, N., Kang, S., Kim, S.Y., Yoo, C. and Lee, J.-S. (2023), "Instrumented dynamic cone penetrometer incorporated with time domain reflectometry", *Measurement*, **206**, 112337. https://doi.org/10.1016/j.measurement.2022.112337
Rhebergen, J.B., Lensen, H.A., Schwering, P.B., Marin, G.R. and Hendrickx, J.M. (2002), "Soil moisture distribution around land mines and the effect on relative permittivity", In: *Detection and Remediation Technologies for Mines and Minelike Targets VII*, Vol. 4742, pp. 269-280. https://doi.org/10.1117/12.479098
Tacim, G., Posluk, E. and Gokceoglu, C. (2023), "Importance of grouting for tunneling in karstic and complex environment (a case study from Türkiye)", *Int. J. Geo-Eng.*, **14**(1), 6. https://doi.org/10.1186/s40703-023-00183-0
Topp, G.C., Davis, J. and Annan, A.P. (1980), "Electromagnetic determination of soil water content: Measurements in coaxial transmission lines", *Water Resour. Res.*, **16**(3), 574-582. https://doi.org/10.1029/WR016i003p00574
Xuan, Y., Luo, M. and Du, G.-F. (2023), "Pipeline defect detection with depth identification using PZT array and time-reversal method", *Smart Struct. Syst., Int. J.*, **32**(4), 253-266. https://doi.org/10.12989/sss.2023.32.4.253
Yu, J.-D., Kim, S.Y. and Lee, J.-S. (2020a), "Variations in velocity and sensitivity of electromagnetic waves in transmission lines configured in model piles with necking defects containing soils", *Sensors*, **20**(22), 6541. https://doi.org/10.3390/s20226541
Yu, J.-D., Lee, J.-S. and Yoon, H.-K. (2020b), "Circular time-domain reflectometry system for monitoring bridge scour depth", *Mar. Geores. Geotechnol.*, **38**(3), 312-321. https://doi.org/10.1080/1064119X.2019.1571131
Yu, J.-D., Lee, J.-S. and Kim, H.-K. (2021), "A hybrid nondestructive testing method for detecting cavities behind the retaining wall", *Smart Struct. Syst., Int. J.*, **28**(4), 567-578. https://doi.org/10.12989/sss.2021.28.4.567